Journal of Vibration Engineering & Technologies (2024) 12:2319–2334
https://doi.org/10.1007/s42417-023-00981-x

ORIGINAL PAPER

Seismic Vulnerability Assessment of RC Frame Buildings Designed Using the DDBD Approach: A Parametric Study

Twinsy N. Palsanawala[1] · Kaushik M. Gondaliya[1] · Vishisht Bhaiya[1] · Sandip A. Vasanwala[1]

Received: 2 February 2023 / Revised: 6 April 2023 / Accepted: 11 April 2023 / Published online: 27 April 2023

Abstract

Direct displacement-based seismic design (DDBD) is widely popular due to the effectiveness of the design approach for achieving the structure's predefined displacement limits. The seismic vulnerability assessment is computed on DDBD-designed structures to anticipate the future state of the structure, which has the potential to enhance the current design. In the present study, 4, 8, and 15-storey reinforced concrete (RC) frame structures are designed using DDBD and force-based design (FBD) under soft, medium, and hard soil conditions. A displacement profile is generated considering life safety (LS) and collapse prevention (CP) performance limits identified as per FEMA 356 (2000). The design response spectra to calculate base shear are taken from the revised IS 1893 Part-1 (2016) at zone-V. The nonlinear multi-mode pushover analysis is performed to investigate RC frame buildings and evaluate RC frames' nonlinear behavior in terms of drift profiles and seismic vulnerability by generating fragility curves. The R factor determined by nonlinear static analysis varies between buildings based on their height, soil conditions, and performance status but is observed to be more than the code-specified number. The estimated level of damage to RC frame structures built on soft soil sites is moderate or between 1.5 and 2.5. Nonetheless, the likelihood of collapse for all studied frames is less than the threshold collapse of 10%.

Keywords Direct displacement-based design · Force-based design · Multi-mode pushover analysis · Fragility curve · R factor · Damage index

Introduction

In many nations, earthquakes have considerable effects on human life and assets. The world economy suffers due to the frequent occurrence of these events, forcing structural engineers and researchers to establish numerous methodologies to sustain the economy and human lives. Priestley & Kowalsky (2000) developed the DDBD method to design structures according to their requirements during seismic circumstances [1]. Displacements are the structure's fundamental response to understanding structural behavior rather than forces. However, displacements have been tested for serviceability limitations after the force-based design procedure. By establishing a maximum displacement limit at the outset and checking for strength at the end, structural engineers may easily predict design needs for significant earthquakes.

Priestley & Kowalsky (2000) proposed the DDBD methodology of performance-based design for buildings to fix the deficiencies and limitations of the conventional method [1]. This technique allows designing a structure to accomplish a specified displacement in the case of a design-level earthquake. The DDBD technique involves multiple phases starting with predicting the seismic deformation of a single degree of freedom system (SDOF) estimated using reports that follow the performance-based design [2]. SDOF system represents the first mode of vibration of the multi-degree of freedom (MDOF) system [3]. Finally, base shear is determined using secant stiffness, rather than assuming initial stiffness, to get more accurate results [4].

✉ Twinsy N. Palsanawala
d20ce033@ced.svnit.ac.in

Kaushik M. Gondaliya
d19am007@amd.svnit.ac.in

Vishisht Bhaiya
vishisht@amd.svnit.ac.in

Sandip A. Vasanwala
sav@amd.svnit.ac.in

[1] Department of Civil Engineering, Sardar Vallabhbhai National Institute of Technology, Surat, Gujarat 395007, India

In earlier studies, building performance is precisely evaluated by examining the dynamic behavior of different moment-resisting RC frames designed using DDBD [5]. The incremental response spectrum analysis, multi-mode pushover analysis, and modal pushover analysis variant are well-developed methods to understand the nonlinear seismic behavior of structure [6, 7]. Before a decade, the building equipped with various foundation isolation systems acquired some interest in DDBD approach [8]. The accumulated dissipative effect of structural damping may become sufficient to affect the dynamic behaviors of building structures manifestly [9]. Various techniques are invented to preserve structures with optimal response parameters [10, 11]. Changing the influence parameters in this manner increases the structure's long-term stability, resulting in outstanding numerical behavior. [12, 13].

A comparison of DDBD with force-based design (FBD) has been conducted by considering base shear, maximum displacement, storey drift evaluation, structural failure mechanism, and damage indices calculations to determine the efficiency [14, 15]. In recent years, the DDBD method has shown advancement in irregular buildings, and guidelines have been generated for setback irregularities [16]. The Indian spectra used to know the seismic performance of various RC frames are designed considering LS performance level [17]. The displacement profiles and equivalent viscous damping are efficient parameters that may be directly incorporated during the design of a structure to achieve realistic simulation are investigated [18]. The most relevant parameters from all are chosen for the current study.

The future probability of a structure's collapse is now the primary concern, which may be determined by generating fragility curves. For a particular seismic event, the representation of the probability of equaling or exceeding a specific damage state of a structure is known as the fragility curve. Kennedy et al. [19] originated fragility curves by considering conditional failure frequency against PGA for a nuclear power plant to evaluate the damage. Recently fragility curves have been widely used for assessing damage states in structures like RC frames [20, 21], elevated water tanks [22], and bridges [23]. Several approaches summarized for fragility analysis are discussed in detail in seismic risk evaluation using various analysis methods [24]. Fragility curves are represented through a standard lognormal distribution function that comprises median and standard deviation [25].

Considering numerous aspects, the functionality of structures under seismic excitation can be predicted after a step-by-step investigation from start to end. In the present study, 4, 8, and 15-storey RC frame structure designs are carried out by applying DDBD, and FBD approaches considering various soil conditions and a maximum considered earthquakes. The displacements in the DDBD approach performed for structures are incorporated for life safety (LS) and collapse prevention (CP) performance limits. The nonlinear static multi-mode pushover study is conducted to account for higher mode effects and calculate the structure's yield and final displacements. The pushover analysis results determine the response reduction factor (R factor) for these structures, which reveals the structure's energy dissipation capability under various conditions. The seismic performance of the studied RC frame is estimated by generating fragility curves and determining the probability of exceedance of a particular damage state at the performance point. The seismic damage index provides a quantitative assessment of structural damage, followed by the structural damage state in the future. Finally, the outcomes of this study contribute to implementing the DDBD approach in Indian building regulations, together with general structural design expertise.

Mathematical Modelling

Materials and Geometry Description

4, 8, and 15-storey RC plan symmetric frame structure situated on soft, medium, and hard soil sites is considered to evaluate RC buildings' performance on various ground motions, as shown in Fig. 1. Each model is categorized as indicated in Table 1 to facilitate identification. The RC frames are designed as special moment resisting fame with code prescribed R factor of 5, fixed-based and ductile detailing is based on IS 13920 (2016) [26] provisions. The building is situated in the most critical zone V (PGA = 0.36 g). Each floor height is 3.2 m, and the bay width is 5.8 m. The structure is subjected to a live load of 3 kN/m^2 on ordinary levels and 1.5 kN/m^2 on the roof floor. The infill wall's dead load is transmitted to a beam with a wall thickness of 230 mm, and the infill masonry wall's density is assumed to be 20 kN/m^3. The slab load is calculated at a thickness of 150 mm and a density of 25 kN/m^3. M30 concrete grade and Fe500 steel grade are used for steel bars. The building models are designed using two distinct approaches: FBD and DDBD, following IS 456 (2000) [27]. As indicated, the drift constraints selected to implement the DDBD approach are 2% and 4% for LS and CP, respectively [2].

FE Modeling

The 3D modeling of RC frame buildings is carried out using the building information modeling solution of MIDAS Gen2021, version 3.1 [29]. The frame elements and their attributes are modeled and assigned by providing material properties and sectional properties to the general beam/tapered beam element type. The vertical loads are converted into masses and are performed as lumped masses, excluding the self-weight of the building.

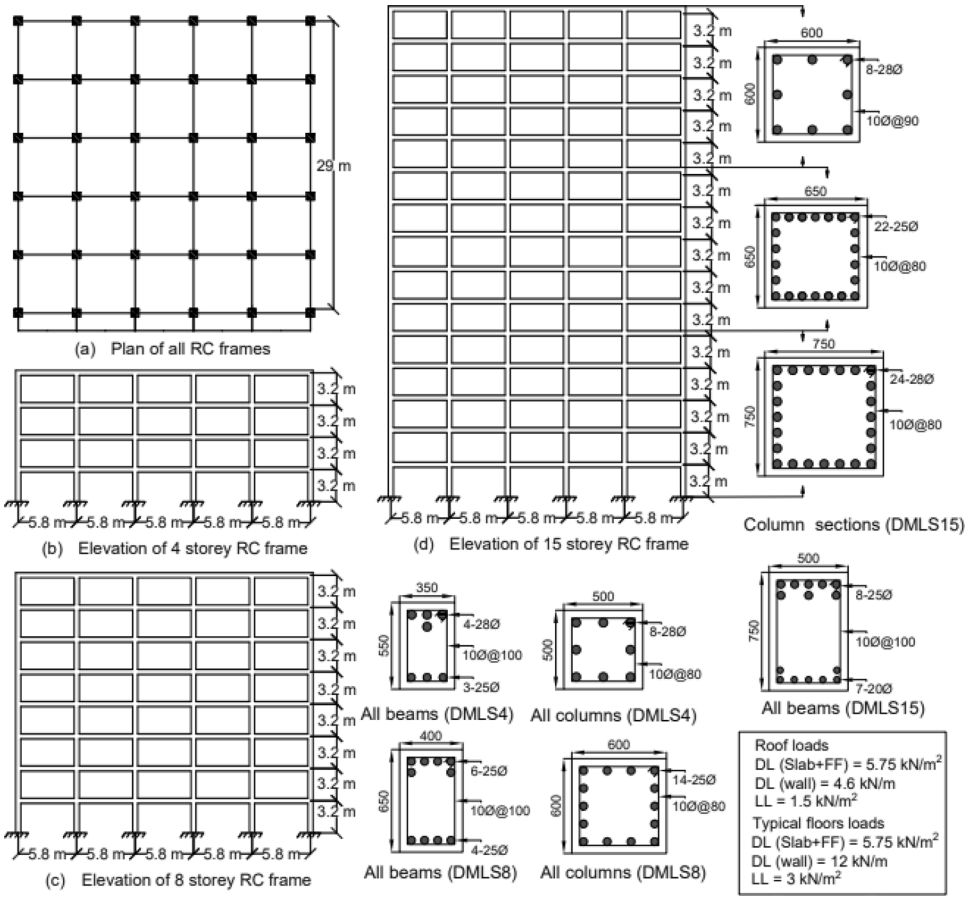

Fig. 1 **a** Plan and elevation of **b** 4-storey **c** 8-storey **d** 15-storey RC frames and section details (in mm) of DMLS models

Table 1 Model IDs of RC frames at various performance levels and soil types

Sr. no	Procedure	Soil type	Performance level	Model ID		
				4-storey	8-storey	15-storey
1	DDBD	Soft	LS	DSLS4	DSLS8	DSLS15
2	DDBD	Soft	CP	DSCP4	DSCP8	DSCP15
3	FBD	Soft	Code-based	FS4	FS8	FS15
4	DDBD	Medium	LS	DMLS4	DMLS8	DMLS15
5	DDBD	Medium	CP	DMCP4	DMCP8	DMCP15
6	FBD	Medium	Code-based	FM4	FM8	FM15
7	DDBD	Hard	LS	DHLS4	DHLS8	DHLS15
8	DDBD	Hard	CP	DHCP4	DHCP8	DHCP15
9	FBD	Hard	Code-based	FH4	FH8	FH15

RC frames 1, 2, 4, 5, 7, 8—The first letter of the model ID indicates the DDBD approach used for lateral load distribution of the RC frame. The second letter indicates the type of soil site used as per IS 1893 Part-1 (2016) [28] to evaluate the time period from the response spectrum, third and fourth letters indicate the performance limit state (*LS* Life safety, *CP* Collapse prevention) used to generate displacement profiles and lastly the number of stories mentioned. RC frames 3, 6, 9-The first letter of the model ID indicates the FBD approach used for the lateral load distribution of the RC frame. The second letter indicates the type of soil used as per IS 1893 Part-1 (2016) [28], and at the end, the number of stories is mentioned

The material's nonlinear behavior is simulated using the MIDAS GSD tool. The concrete nonlinearity is modeled using the Mander model's constitutive stress–strain curve [30], and the nonlinear behavior of the steel is determined using the Park strain hardening model [31], as shown in Fig. 2.

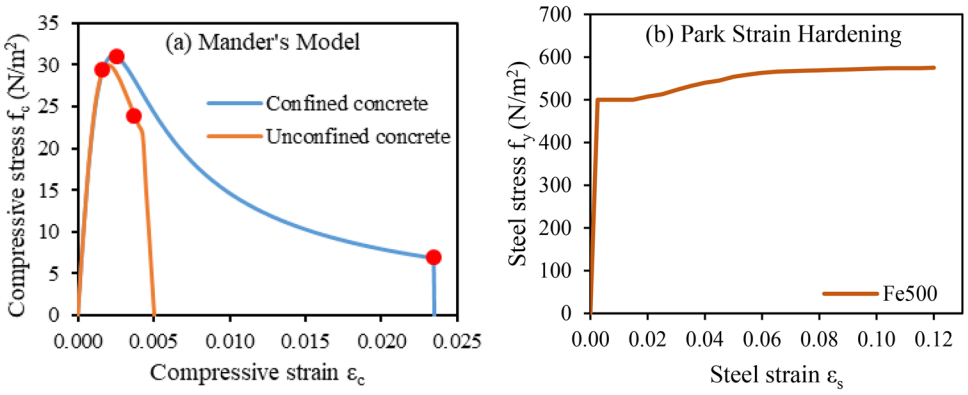

Fig. 2 Nonlinear material models of **a** concrete and **b** steel

DDBD and FBD Approach

Shabita & Sozen [3] proposed a linear model for evaluating nonlinear response ranges, which serves as the foundation for the DDBD approach. The DDBD approach describes the procedures involved in constructing a structure to accomplish rather than be constrained by a predefined displacement when subjected to a design-level earthquake. Priestley et al. [32] describe the methodology of the DDBD approach adopted in this research as an overall framework that may be used for any structure. The DDBD approach begins with transforming an MDOF system into an SDOF system, which gives a similar response shown in Fig. 3a. In the second stage, the maximum reaction of an SDOF system is represented by a secant stiffness (K_e) at the predetermined design displacement (Δ_d) (Fig. 3b). The design displacement is established at the commencement of the process, considering performance limits, ductility demands, or material strains. In the third stage, equivalent viscous damping (ξ_{eq}) is obtained by calculating the displacement ductility demand at the design displacement (Fig. 3c). Furthermore, the final step determines the effective time period at design displacement using displacement spectra following Indian codal requirements (Fig. 3d).

Steps involved in the DDBD approach computing lateral load distribution for RC frame building [32]:

1. Design displacement evaluation (Δ_d)

At the start of the procedure, the design displacement of the structure is estimated by specifying a specific performance limit, as described previously. The displacement

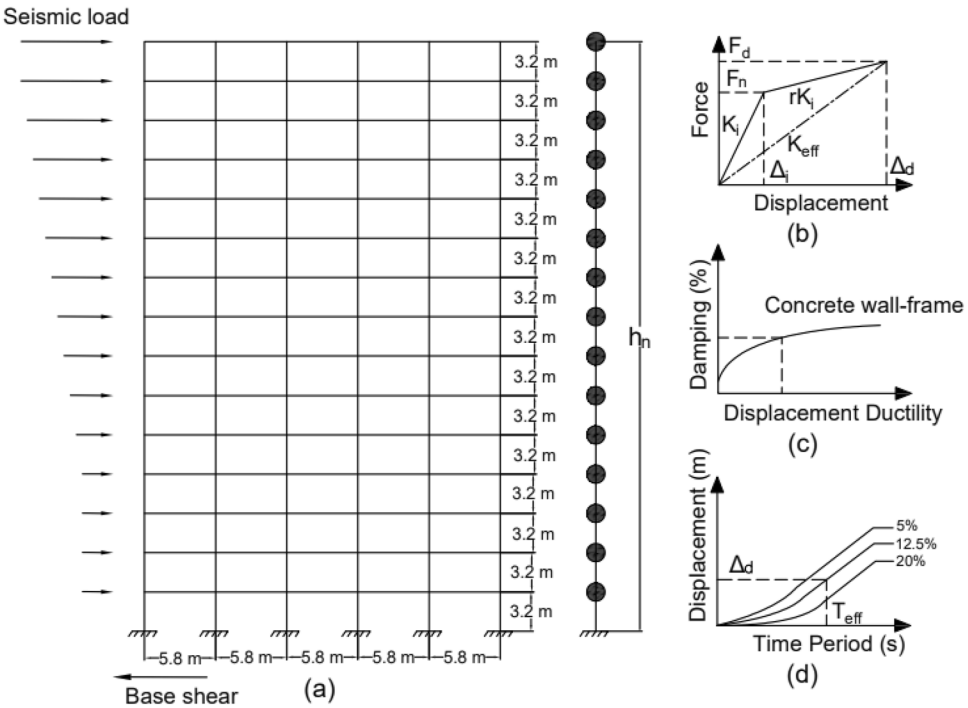

Fig. 3 Phases of the DDBD approach [1]

of each storey (Δ_i) is determined considering the mode shapes (δ_i) given in Eqs. (2–3), which is multiplied by the critical displacement (Δ_c) at the first mode shape obtained by the design drift limits as specified in FEMA 356 (2000) [2].

$$\Delta_i = \delta_i \left(\frac{\Delta_c}{\delta_c} \right) \tag{1}$$

$$\delta_i = \frac{h_i}{h_n} \quad \text{for } n \le 4 \tag{2}$$

$$\delta_i = \frac{4}{3}\left(\frac{h_i}{h_n}\right)\left(1 - \frac{h_i}{h_n}\right) \quad \text{for } n > 4 \tag{3}$$

where *n* denotes the number of stories, h_i denotes the height of the ith storey, h_n indicates the total height of a building. For buildings having several stories, more than ten, to consider the higher mode effect, Eq. (1) is multiplied by the drift reduction factor ω_θ (Eq. (4)).

$$\omega_\theta = 1.15 - 0.0034 H_n \le 1.0 \tag{4}$$

Now, the design displacement (Δ_d) of the substitute structure is calculated from Eq. (5)

$$\Delta_d = \frac{\sum_{i=1}^{n} (m_i \Delta_i^2)}{\sum_{i=1}^{n} (m_i \Delta_i)} \tag{5}$$

2. Determination of the effective mass (m_{eff}) and the effective height (h_{eff})

The effective mass (m_{eff}) and the effective height (h_{eff}) of the RC frame are calculated using equations (6, 7).

$$m_{eff} = \frac{\sum_{i=1}^{n} (m_i \Delta_i)}{\Delta_d} \tag{6}$$

$$h_{eff} = \frac{\sum_{i=1}^{n} (m_i \Delta_i H_i)}{\sum_{i=1}^{n} (m_i \Delta_i)} \tag{7}$$

where m_i denotes the i^{th} storey mass.

3. Determination of ductility demand (μ)

Ductility demand is evaluated by calculating yield rotation (θ_y) and yield displacement (Δ_y) using Eqs. (8, 9)

$$\Delta_y = \theta_y * H_e \tag{8}$$

$$\theta_y = 0.5 * \varepsilon_y * \left(\frac{L_b}{H_b} \right) \tag{9}$$

where ε_y denotes the yield strain of steel, L_b denotes the beam length, and H_b represents the beam depth. Then design ductility demand is found by the ratio between the design and yield displacement (Eq. (10)).

$$\mu = \frac{\Delta_d}{\Delta_y} \tag{10}$$

4. Determination of equivalent viscous damping (ξ_{eq})

Equation (11) gives the equivalent viscous damping (ξ_{eq}) from the ductility demand (μ). The equivalent viscous damping is multiplied with the damping correction factor as per 1893 Part-1 (2002) [33]. The interpolation method is used to find the exact value of the damping modification factor for the specific damping.

$$\xi_{eq} = 5 + 120\left(\frac{1 - \mu^{-0.5}}{\pi}\right)\% \tag{11}$$

5. Determination of the effective time period (T_{eff}) of the SDOF structure

Figure 4(a) displayed the displacement spectra generated from acceleration spectra for 5% damping. The effective period of the SDOF structure at peak displacement response is determined by entering the design displacement of the substitute SDOF structure Δ_d and obtaining

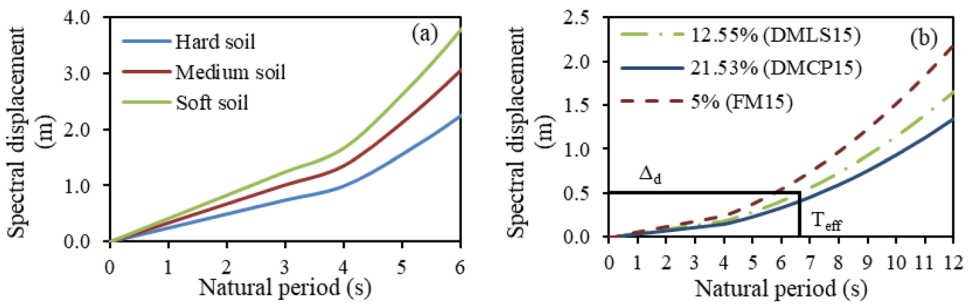

Fig. 4 **a** Displacement spectra of various soil types and **b** Damped spectra of medium soil for zone V

the effective period T_{eff} from damped response spectra of different models for a critical zone (Fig. 4(b)).

6. Determination of the effective stiffness (K_{eff}) and the design base shear (V_b) of the SDOF structure

From the effective time period and the effective mass, the effective stiffness is obtained by Eq. (12), multiplying the effective stiffness (K_{eff}) with design displacement (Δ_d), and the design base shear (V_b) is evaluated using Eq. (13).

$$K_{eff} = \frac{4\pi^2 m_{eff}}{T_{eff}^{\ 2}} \tag{12}$$

$$V_b = K_{eff} * \Delta_d \tag{13}$$

7. Determination of lateral load distribution (Q_i) at each storey

The lateral loads have been distributed at a different storey for RC frames using design base shear given by Eqs. (14, 15),

$$Q_i = V_b \frac{m_i \Delta_i}{\sum_{i=1}^{n} (m_i \Delta_i)} \quad \text{for } n \le 10 \tag{14}$$

$$Q_i = Q_t + 0.9 V_b \frac{m_i \Delta_i}{\sum_{i=1}^{n} (m_i \Delta_i)} \quad \text{for } n > 10 \tag{15}$$

where $Q_t = 0.1V_b$, Q_t is a lateral load at the roof level. Table 2 summarizes an example computation of the above-discussed process using DMLS15 as an illustration model.

Table 2 The sample calculation of lateral load distribution using DDBD for the building Model DMLS15

Level	h_i	m_i (t)	δ_i	Δ_i (m)	$m_i\Delta_i$ (t.m)	$m_i\Delta_i^2$ (t.m^2)	$m_i\Delta_i h_i$ (t.m^2)	Qi (kN)
15	48.00	986.96	1.00	0.71	703.71	501.74	33,777.85	1271.24
14	44.80	1255.75	0.95	0.68	854.23	581.10	38,269.58	689.42
13	41.60	1255.75	0.91	0.65	810.46	523.07	33,715.09	654.09
12	38.40	1255.75	0.85	0.61	764.03	464.86	29,338.88	616.62
11	35.20	1255.75	0.80	0.57	714.95	407.06	25,166.41	577.01
10	32.00	1271.00	0.74	0.53	671.28	354.53	21,480.85	541.76
9	28.80	1286.25	0.68	0.48	623.62	302.36	17,960.39	503.30
8	25.60	1286.25	0.62	0.44	565.20	248.36	14,469.18	456.15
7	22.40	1286.25	0.55	0.39	504.06	197.54	11,291.00	406.81
6	19.20	1286.25	0.48	0.34	440.21	150.66	8451.95	355.27
5	16.00	1314.32	0.41	0.29	381.79	110.90	6108.56	308.12
4	12.80	1342.39	0.33	0.24	317.62	75.15	4065.57	256.34
3	9.60	1342.39	0.25	0.18	242.47	43.80	2327.72	195.69
2	6.40	1342.39	0.17	0.12	164.48	20.15	1052.69	132.75
1	3.20	1342.39	0.09	0.06	84.78	5.35	271.29	68.42
Σ				6.30	7842.90	3986.63	247,747.01	7033.02

Table 3 The parametric details of 15-storey building Models obtained considering the DDBD approach

Parameter	DSLS15	DSCP15	DMLS15	DMCP15	DHLS15	DHCP15
h_n [m]	48	48	48	48	48	48
W [MN]	195.24	195.24	187.40	187.40	181.10	181.10
δ_c	0.09	0.09	0.09	0.09	0.09	0.09
ω_θ	0.9868	0.9868	0.9868	0.9868	0.9868	0.9868
Δ_d [m]	0.509	1.018	0.508	1.017	0.507	1.014
Δ_y [m]	0.306	0.306	0.327	0.327	0.351	0.351
μ	1.66	3.33	1.55	3.11	1.44	2.89
m_{eff} [t]	16,099.18	16,099.18	15,429.35	15,429.35	14,899.05	14,899.05
K_{eff} [kN/m]	17,236.21	7123.25	13,836.07	5604.90	10,171.06	4046.39
T_{eff} [s]	6.07	9.44	6.64	10.42	7.60	12.00
V_b [kN]	8773.79	7251.92	7033.02	5698.06	5159.11	4104.94
V_b/W [%]	4.49	3.71	3.75	3.04	2.85	2.27

Table 3 shows the parametric detail evaluated from the DDBD approach of 15-storey models.where, h_n represents the height of the roof from the base, W represents the total seismic weight of the RC frame building, δ_c represents critical normalised mode shape, ω_θ represents drift reduction factor, Δ_d represents design displacement, Δ_y represents yield displacement, μ represents displacement ductility, m_{eff} represents effective mass, K_{eff} represents effective stiffness, T_{eff} represents effective time-period, V_b represents base shear, and V_b/W represents Percentage of lateral force.

The force-based approach is widely applied during structure design, and Indian practice norms are entirely based on this approach. The working stress, the ultimate stress method, and the limit state method come under the category of FBD. The most recent procedure is the limit state method, which encompasses both the limit state of serviceability and strength. When studying any structure utilizing the limit state method, the designer evaluates the linear relationship between stress and strain. The analysis and design are limited to the elastic range of the material property. Specific measures are included in the code of practice to ensure that structures behave in the plastic content of material properties in the event of lateral loads induced by earthquakes. However, this method cannot predict damage to structural components and actual performance in the plastic range. Additionally, regardless of soil conditions, the R factor remains the same for all special moment resisting frames.

In code-based FBD, the design base shear (V_b), as calculated as per IS 1893 Part-1 (2016) [28], shall be distributed along the height of the building using Eq. (16).

$$Q_i = V_b * \frac{W_i h_i^2}{\sum_{i=1}^{n} W_i h_i^2} \tag{16}$$

where Q_i = Design lateral force at floor i, W_i = Seismic weight of floor i, h_i = height of floor i measured from the base, n = number of stories. The rebar detailing the studied study RC frame building models is shown in Table 4 and Table 5. Only for 15-storey buildings, variation in column dimensions with height is considered for optimal structural design. The time period considered for the RC frame is calculated as per Eq. (17), Where h = height of RC frame building.

$$T = 0.075h^{0.75} \tag{17}$$

Table 4 Reinforcement details of 4-storey and 8-storey RC frame models

Members	Models	Width (mm)	Depth (mm)	Reinforcement details (in mm)		Models	Width (mm)	Depth (mm)	Reinforcement details (in mm)	
				Top	Bottom				Top	Bottom
Beams	DSLS4	350	550	5-28Φ	5-20Φ	DSLS8	400	650	7-25Φ	7-20Φ
Columns		500	500	10-28Φ*			600	600	14-28Φ*	
Beams	DSCP4	350	550	5-25Φ	3-25Φ	DSCP8	400	650	5-28Φ	4-25Φ
Columns		500	500	8-28Φ*			600	600	14-25Φ*	
Beams	FS4	350	550	6-25Φ	7-16Φ	FS8	400	650	7-25Φ	4-25Φ
Columns		500	500	12-25Φ*			600	600	12-28Φ*	
Beams	DMLS4	350	550	4-28Φ	3-25Φ	DMLS8	400	650	6-25Φ	4-25Φ
Columns		500	500	8-28Φ*			600	600	14-25Φ*	
Beams	DMCP4	350	550	4-25Φ	4-20Φ	DMCP8	400	650	5-25Φ	8-16Φ
Columns		500	500	8-25Φ*			600	600	12-25Φ*	
Beams	FM4	350	550	5-25Φ	7-16Φ	FM8	400	650	6-25Φ	3-28Φ
Columns		500	500	10-25Φ*			600	600	10-28Φ*	
Beams	DHLS4	350	550	3-28Φ	6-16Φ	DHLS8	400	650	5-25Φ	5-20Φ
Columns		500	500	8-25Φ*			600	600	10-28Φ*	
Beams	DHCP4	350	550	3-25Φ	4-16Φ	DHCP8	400	650	4-25Φ	4-20Φ
Columns		500	500	6-28Φ*			600	600	8-28Φ*	
Beams	FH4	350	550	3-28Φ	5-16Φ	FH8	400	650	5-25Φ	5-20Φ
Columns		500	500	8-25Φ*			600	600	12-25Φ*	

*represents uniformly distributed bars

Φ represents the diameter of the bars

Table 5 Reinforcement details of 15-storey RC frame models

Members	Floors	Width (mm)	Depth (mm)	Models	Reinforcement details (in mm)		Models	Reinforcement details (in mm)		Models	Reinforcement details (in mm)	
					Top	Bottom		Top	Bottom		Top	Bottom
Beams	1–15	500	750	DSLS15	7-28Φ	8-20Φ	DMLS15	8-25Φ	7-20Φ	DHLS15	7-25Φ	5-20Φ
Columns	1–5	750	750		26-28Φ*			24-28Φ*			26-25Φ*	
	6–10	650	650		24-25Φ*			22-25Φ*			16-28Φ*	
	11–15	600	600		10-28Φ*			8-28Φ*			8-25Φ*	
Beams	1–15	500	750	DSCP15	8-25Φ	7-20Φ	DMCP15	7-25Φ	8-16Φ	DHCP15	6-25Φ	5-16Φ
Columns	1–5	750	750		24-28Φ*			26-25Φ*			22-25Φ*	
	6–10	650	650		22-25Φ*			16-28Φ*			20-25Φ*	
	11–15	600	600		10-25Φ*			8-25Φ*			8-25Φ*	
Beams	1–15	500	750	FS15	7-28Φ	8-20Φ	FM15	8-25Φ	10-16Φ	FH15	6-28Φ	7-16Φ
Columns	1–5	750	750		26-28Φ*			28-25Φ*			20-28Φ*	
	6–10	650	650		18-28Φ*			22-25Φ*			16-28Φ*	
	11–15	600	600		12-25Φ*			10-25Φ*			8-25Φ*	

*represents uniformly distributed bars

Φ represents the diameter of the bars

Plastic Hinge Formation

Moment-rotation (M-θ) type plastic hinge model is applied to incorporate nonlinear behavior using the MIDAS Gen2021, v3.1 [29] software as per ASCE 41 (2017) [34]. The skeleton model used to perform the nonlinear analysis is an empirical hysteresis model, characterizing inelastic hysteresis behaviors. The axial component is represented by a central spring, while the two translational components are represented by two springs at either end, with force–displacement relationships. The two flexural components, M_y and M_z, are represented by springs defined by the connection between the moment and rotation angle. For beam elements, coupled axial force–uniaxial moment behavior is observed by computing the flexural yield strength of a hinge while considering the influence of axial force (P-M). For column elements, coupled axial force-biaxial moment behavior is seen by computing the flexural yield strength of a hinge while taking axial force into account (P-M-M). While locating lumped inelastic hinges, the axial component of a member is affixed to its center. However, both ends are selected for the bending moment components. The modeling criteria and acceptance parameters for beams and columns hinges of RC frame structures are taken as per ASCE 41 (2017) [34].

Multi-mode Pushover Analysis

Earthquake loads are stochastic in nature [35]. This study addresses stochastic loads as lateral design loads, which are incrementally applied until the individual components of a structure yield or buckle. Nonlinear static analysis is a static nonlinear procedure to quantify the nonlinear performance of designed building structures under lateral loading. The influence of higher-mode effects on the structural and nonstructural seismic performance of RC frame structures

Table 6 Modal analysis results of 15-storey RC frame models

Models	Model period T (s)			Cumulative mass participation (%)		
	Mode 1	Mode 2	Mode 3	Mode 1	Mode 2	Mode 3
DSLS15	2.406	0.829	0.482	77.55	88.10	92.22
DSCP15	2.692	0.936	0.545	76.36	87.20	91.51
FS15	2.413	0.832	0.483	77.55	88.08	92.22
DMLS15	2.592	0.845	0.492	76.36	87.44	91.51
DMCP15	2.798	1.064	0.612	74.20	85.67	90.51
FM15	2.693	0.920	0.544	76.36	87.20	91.51
DHLS15	2.732	0.954	0.563	75.76	86.39	90.98
DHCP15	3.011	1.090	0.640	73.76	85.39	90.40
FH15	2.844	0.989	0.612	74.97	86.71	90.82

having a time period greater than one is incorporated by applying multi-mode pushover analysis. A significant number of modes must be considered to capture at least 90% of a structure's mass involvement to comprehend nonlinear behavior (Table 6). The following are the steps involved in multi-mode pushover analysis [6, 36] from the expansion of the modal pushover analysis [37]:

- The structure is first analyzed using static pushover analysis in which monolithically increasing lateral loads are applied until the desired displacement is achieved under constant gravity loads. The lateral load pattern on each node is given by the following Eq. (18).

$$F_n = m\Phi_n \tag{18}$$

The peak value of the roof's movement due to n^{th} mode (u_{rn}) when the high-rise building is pushed is taken from the equation (19),

$$u_{rn} = \Gamma_n \Phi_{rn} D_n \tag{19}$$

- The pushover curve in each mode is then transformed into the capacity curve of the corresponding SDOF system using the modal conversion parameters derived from the same linear (starting) mode shapes [2].
- Peak inelastic response values of interest, including inelastic displacement, the storey drifts, and plastic hinge rotations, are calculated separately for each mode. The square root of the sum of squares (SSRS) formula is used to estimate the combined peak response values. Figure. 5 represents the drift profiles produced from multi-mode pushover analysis of DSLA15, DMLS15, and DHLS15 and drifts generated after SRSS for all building models. RC frames designed using the DDBD approach are well observed within limits for all assessed performance limit states.

The value of the design base shear and drifts at performance points calculated using the DDBD follow the same

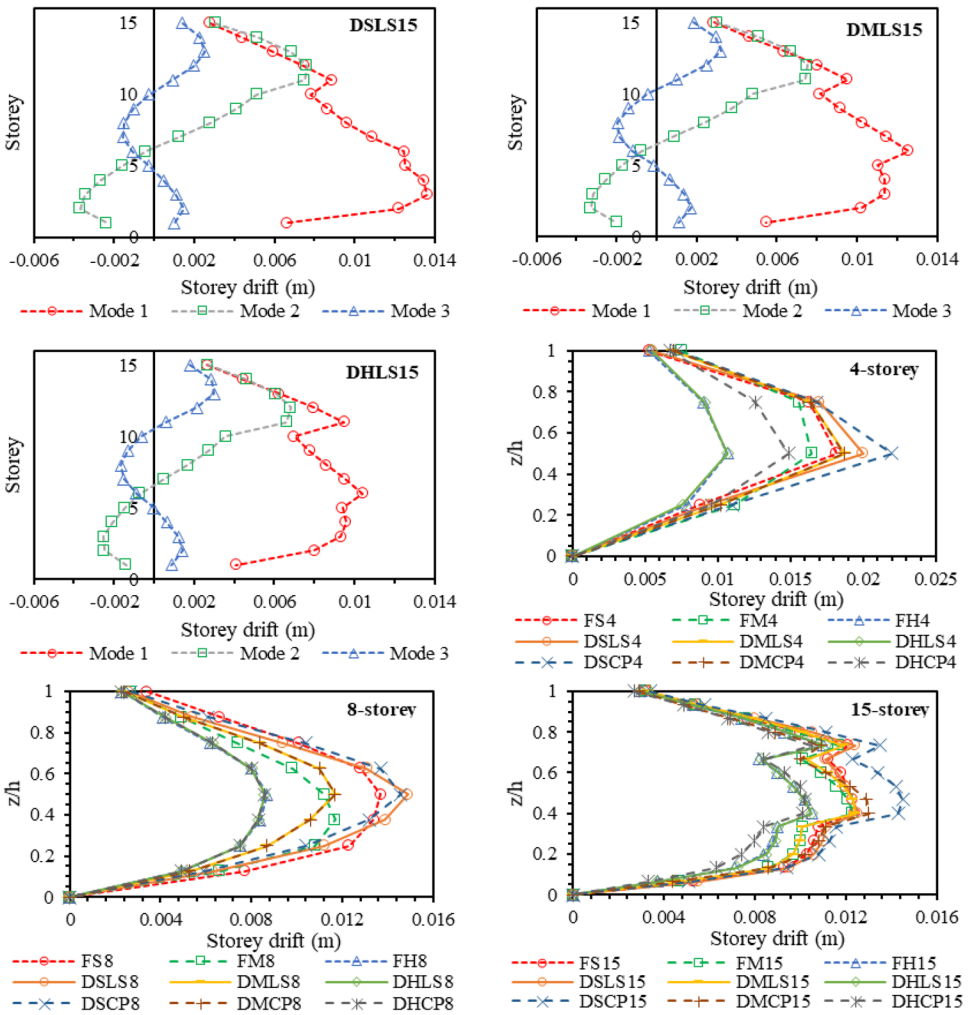

Fig. 5 Drift profiles of all participating modes, along with mean drift comparison of various models

pattern (Table 3 & Fig. 5). The base shear values obtained by the FBD approach range between the base shear values generated by the LS and CP performance limitations in the DDBD approach, but the values are slightly nearer to the LS performance criteria revealing that Indian codes design structures are nearer to the 2% drift limit criteria specified in the DDBD approach.

The nonlinear behavior of RC frame buildings is evaluated by generating pushover curves implementing the multi-mode pushover analysis. The pushover curves represent the base shear v/s top displacement graph covering the entire range of structural behavior from linear to yielding, nonlinear, and up to collapse of structures. The inter-storey drift from multi-mode pushover analysis at performance points evaluated for LS models is observed to be less than 2%, i.e., $0.02 \times 3.2 = 0.064$ m, except DSLS4 and the values for CP models are observed to be less than 4%, i.e., $0.04 \times 3.2 = 0.128$ m, indicating that the DDBD method is effectively implemented. The RC frame buildings constructed on soft soil observed the maximum inter-storey drift, whereas RC frame buildings constructed on hard soil observed the minimum inter-storey drift.

The plastic hinge development in both design approaches due to seismic loading shows ductile behavior in the nonlinear zone. After the first yielding, plastic hinges began to form in the beam elements in both design approaches due to the adopted strong-column weak-beam philosophy. As yielding continues, plastic hinges in beams increase and column hinges begin forming, indicating a substantial degree of energy dissipation in the elements. A backbone curve arises as the building achieves its load-bearing limit and begins to form collapse hinges. In all the models, sufficient ductility is observed, which will help in preventing column failure caused by flexure and shear.

Figure 6 demonstrates the capacity curve of 15-storey RC frames generated after performing nonlinear static analysis. Compared to FBD, the elastic stiffness (load deflection ratio in an elastic zone) of structures developed using DDBD at the LS performance level is considerably greater. However,

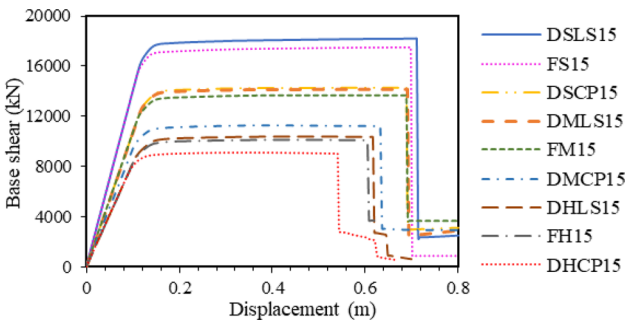

Fig. 6 The capacity curves/pushover curves of 15-storey building models

models designed using CP performance exhibit less elastic stiffness than FBD, with soft soil having the most significant base shear values and hard soil the lowest. If we consider the medium soil condition, the nonlinear behavior observed for FM15 and DMCP15 reveals a significant difference in ultimate displacement, but the difference between DMLS15 and FM15 is negligible. Based on the abovementioned criteria, models designed using the FBD approach are closer to those designed considering LS performance criteria but have a higher capacity than those designed with CP performance criteria. 4-storey and 8-storey RC frame structures behave identically under lateral loads.

Seismic Assessment Parameters

Response Reduction Factor (R Factor)

The R factor represents the amount of energy dissipated during an earthquake after yielding. The R factor for a special moment resisting frame is 5, according to the Indian code [28]. In this study, a specific model's R factor values are derived from a structure's performance and compared with code-based R factor values. The procedure to determine the R factor based on a building's performance is described in ATC 19 [38]. The technique is applied to numerous constructions to evaluate the inelastic nature all around the globe [39–41]. The R factor evaluation from various factors is presented by Eq. (20).

$$R = R_s \times R_\mu \times R_\zeta \times R_R \tag{20}$$

where R_s is the strength factor calculated from the ultimate shear and the design base shear ratio. R_μ is the ductility factor derived from the performance characteristics of yield displacement and ultimate displacement of the structure,

R_ζ and R_R are the ductility and redundancy factors, respectively, and both have a value of 1. [22, 38]

Table 7 gives the R factor values of studied models and shows that the performance limit and soil conditions influence the values of R and its components. The strength component governs the R factor in 4-storey RC frames, whereas the ductility factor governs the R factor in 15-storey RC frames. The R values for various soil properties RC frame analyses developed based on DDBD and FBD for seismic zone-V are observed from 4.98 to 10.86. R factors observed for structures constructed using the FBD approach for 4 and 8 stories are incredibly close to or slightly over the code-specified value of 5, indicating that the Indian code provides a safer design [28]. For 15-storey RC frames, more prominent R factors are recorded. The FS15 model has a 12.57% higher R factor value than the FH15 model.

For the design of structures utilizing the DDBD approach, the R factor values increase as the soil changes from soft to

Table 7 R factor values derived considering various factors

Model ID	V_d (kN)	V_u (kN)	Δ_y (m)	Δ_u (m)	$R_\mu = \frac{\Delta_u}{\Delta_y}$	$R_s = \frac{V_u}{V_d}$	*R*
DSLS4	3221	6717	0.036	0.153	2.74	2.09	5.71
DSCP4	1722	6461	0.039	0.162	2.70	3.75	10.14
FS4	3950	8374	0.040	0.179	2.82	2.12	5.98
DMLS4	2260	6336	0.054	0.165	2.26	2.80	6.34
DMCP4	1384	6335	0.054	0.165	2.26	4.58	10.35
FM4	3879	8203	0.048	0.157	2.35	2.11	4.98
DHLS4	1302	5339	0.056	0.165	2.21	4.10	9.07
DHCP4	993	5020	0.057	0.16	2.15	5.06	10.86
FH4	2987	6623	0.051	0.157	2.27	2.22	5.04
DSLS8	4392	9824	0.110	0.384	2.45	2.24	5.47
DSCP8	3537	8251	0.100	0.39	2.61	2.33	6.08
FS8	6802	14,407	0.086	0.387	2.82	2.12	5.98
DMLS8	3642	8428	0.096	0.394	2.68	2.31	6.21
DMCP8	2862	8287	0.092	0.406	2.80	2.90	8.10
FM8	5496	11,742	0.088	0.397	2.83	2.14	6.05
DHLS8	2592	7849	0.086	0.402	2.89	3.03	8.75
DHCP8	1997	7108	0.092	0.402	2.78	3.56	9.90
FH8	3780	8703	0.100	0.382	2.58	2.30	5.93
DSLS15	8773	16,001	0.163	0.71	4.36	2.08	7.94
DSCP15	7251	13,215	0.179	0.688	3.84	1.97	7.00
FS15	8580	15,985	0.156	0.694	4.45	2.04	8.29
DMLS15	7033	14,598	0.179	0.691	3.86	2.01	8.01
DMCP15	5698	11,238	0.152	0.632	4.16	1.97	8.20
FM15	6707	13,674	0.163	0.688	4.22	2.04	8.61
DHLS15	5159	11,337	0.162	0.615	3.80	2.00	8.34
DHCP15	4104	9011	0.144	0.54	3.75	2.20	8.23
FH15	4766	10,115	0.162	0.605	3.73	2.12	7.93

hard for each limit state. The values of the R factor for the CP performance state are the greatest compared to other performance criteria, which is not unreasonable given that structures constructed for CP performance are intended to withstand greater displacements. There are no provisions for structural design based on performance limit criteria in the Indian code. Thus, the study recommended that the code-specified unique R not be used for all RC frame structures, regardless of performance restrictions.

Fragility Curve Fitting

The probability of exceeding a particular damage state under specific ground motion is derived by generating fragility curves from pushover curves using Eq. (21) [42]. Building performance should be known at the initial stage in plotting the fragility curve. The capacity spectrum method (CSM) is used to evaluate building performance. The performance point of the RC frame is found for each mode by intersecting the capacity curve with the demand curve as per ATC 40 (1996) and FEMA P58-1 (2018) [43, 44].

$$P_{k\text{-}}(S_{di}) = P\left[DS \geq DS_k | S_d\right] = \Phi\left[\frac{1}{\beta_k} \ln\left(\frac{S_d}{S_{d,ds}}\right)\right] \tag{21}$$

where S_d represents the spectral displacement of the capacity curve developed in order to comprehend nonlinear structural behavior, $S_{d,ds}$ represents the median value of S_d, and S_k represents the threshold limit which is specified in Table 8 [25], β_k represents the standard deviation for a given damage

Table 8 More likely damage states, damage state threshold and corresponding mean damage index intervals [19]

More likely damage state	Damage state threshold	Mean damage index intervals
No damage (Sd_0)	–	0.0–0.5
Slight (Sd_1)	0.7*(S_{dy})	0.5–1.5
Moderate (Sd_2)	S_{dy}	1.5–2.5
Severe (Sd_3)	S_{dy} + 0.25 * (S_{du}—S_{dy})	2.5–3.5
Complete (Sd_4)	S_{du}	3.5–4.0

Table 9 Parameter describing the fragility curves and performance point as per FEMA P58-1 (2018) [44]

Model ID	S_{dy} (mm)	S_{du} (mm)	$S_{d,ds}$ (mm)	Spectral displacement (S_d)				Uncertainty (β)			
				S_{d1}	S_{d2}	S_{d3}	S_{d4}	β_1	β_2	β_3	β_4
DSLS4	28	134	43.48	20	28	55	134	0.40	0.58	0.73	0.85
DSCP4	41	196	48.22	29	41	80	196	0.40	0.59	0.73	0.86
FS4	27	151	37.90	19	27	58	151	0.44	0.68	0.79	0.92
DMLS4	34	137	40.52	24	34	60	137	0.37	0.50	0.66	0.78
DMCP4	35	137	40.52	25	35	60	137	0.37	0.49	0.64	0.77
FM4	38	127	39.66	26	38	60	127	0.35	0.44	0.59	0.70
DHLS4	36	137	33.85	25	36	61	137	0.36	0.48	0.64	0.76
DHCP4	35	193	33.88	24	35	74	193	0.43	0.66	0.76	0.93
FH4	47	193	36.48	33	47	83	193	0.37	0.52	0.67	0.80
DSLS8	66	298	74.54	46	66	124	298	0.39	0.56	0.70	0.84
DSCP8	64	304	75.80	44	64	124	304	0.40	0.59	0.72	0.86
FS8	58	302	62.11	41	58	119	302	0.42	0.62	0.73	0.90
DMLS8	58	312	61.28	40	58	121	312	0.42	0.65	0.77	0.91
DMCP8	62	322	63.51	43	62	127	322	0.42	0.63	0.75	0.90
FM8	57	308	54.56	40	57	120	308	0.42	0.65	0.75	0.92
DHLS8	71	355	54.52	50	71	142	355	0.41	0.61	0.74	0.88
DHCP8	71	355	54.52	50	71	142	355	0.41	0.61	0.74	0.88
FH8	75	340	55.63	53	75	141	340	0.39	0.56	0.70	0.84
DSLS15	97	526	108.56	68	97	204	526	0.43	0.65	0.76	0.91
DSCP15	104	507	117.26	73	104	204	507	0.41	0.60	0.72	0.87
FS15	95	516	106.72	66	95	200	516	0.43	0.65	0.77	0.91
DMLS15	101	509	103.15	71	101	203	509	0.41	0.61	0.73	0.89
DMCP15	98	468	102.76	68	98	190	468	0.40	0.59	0.73	0.85
FM15	97	507	101.45	68	97	199	507	0.42	0.63	0.75	0.90
DHLS15	97	448	88.27	68	97	185	448	0.39	0.57	0.71	0.84
DHCP15	88	394	83.73	62	88	165	394	0.38	0.55	0.70	0.83
FH15	97	440	87.67	68	97	183	440	0.39	0.56	0.71	0.83

$S_{d,ds}$ represents displacement at the performance point

state, Φ represents the standard normal cumulative distribution function.

The least-square approach is then utilized to fit the fragility curves [45–47]. Nonetheless, some literature [48] has successfully utilized the HAZUS [49] technique to fit buildings' fragility curves. Table 9 illustrates the estimated uncertainty factor β_k, damage state threshold values, and mean spectral displacement at seismic forces equivalent to.

MCE for seismic zone-V. In addition, it is assumed that the expected damage state, as indicated by the inelastic spectral displacement S_d, follows the binomial probability distribution as given in Eq. (22).

$$P_k = P(DS = DS_k) = P_k(N, d) = \sum_{k=0}^{n-1} \binom{n-1}{k} d^k (1-d)^{n-1-k}; k = 0, 1, 2, \ldots .(N-1) \tag{22}$$

In this study, the damage grades are designated by N, equal to 5. The value of d indicates the amount of damage, ranging from 0 to 1. d = 0 shows no damage to a building. However, the number d = 1 implies that a frame has sustained total damage. Therefore, Eq. (21) is fitted to the acquired point using Eq. (22) and the least-squares principle. Figure 7 displays fragility curves developed using this approach with a fixed probability of 50%. Using the generated fragility curves, the probability of occurrence (P_k) for each damage state is derived by subtracting the acceptable likelihood of subsequent damage state exceedance according to the following Eq. (23):

$$P_k = P_k(k+1) - P_k(k) \tag{23}$$

The fragility evaluation's reliability depends on the optimal values of the uncertainty factor (β) and the

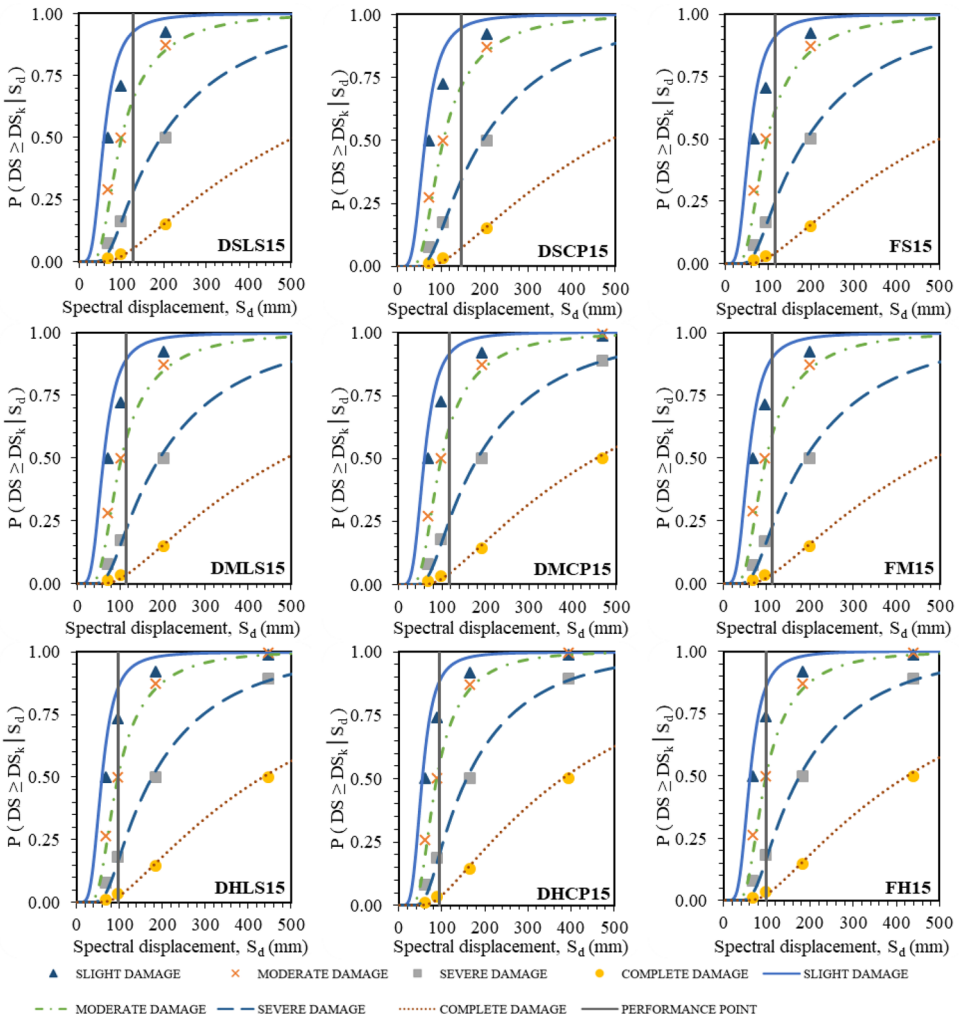

Fig. 7 Fragility curves fitting for 15-storey models considering damage states

threshold limit values for the various predefined damage states [42]. The uncertainty can be classified as aleatory (random variability) and epistemic (resulting from incomplete knowledge); i.e., manufacturing, construction inaccuracy, and seismic hazard can be reduced using uncertainty factor (β). Equation (24) estimates a fragility function for the optimal uncertainty beta ($\widehat{\beta}$) by minimizing the sum of squared error (SSE) between normal and binomial distribution.

$$\widehat{\beta} = \underset{\beta}{\operatorname{argmin}} \sum_{j=1}^{m} \left[P_k(S_{di}) - \sum_{k=0}^{n} kP_k(N,d) \right]^2 \tag{24}$$

S_{dy} represents yield spectral displacement, and S_{du} represents an ultimate spectral displacement.

Seismic Vulnerability Calculating Mean Damage Index

The seismic vulnerability is derived in terms of the mean damage index (DS_m), which is evaluated from the probability of occurrence of each damage state (Eq. (23)). Using a single metric known as the weighted mean damage index (DS_m), the building's most likely damage condition may be described (Eq. (25)).

$$DSm = \sum_{i=1}^{4} kp_k[N,d] \tag{25}$$

where $k = 0$, 1, 2, 3, or 4 depends on the damage state k considered, p_k [N, d] = occurrence probabilities of the given damage state. The mean damage index is weighed to examine the structure's damaged condition. DS_m represents a possible damaged state of a building during a given seismic hazard. For instance, $DS_m = 1.0$ indicates the most likely damage state of the facility would be slight.

Table 10 Probability of exceedance of particular damage state, mean damage index (DS_m), and most likely damage state of RC frame models

Model ID	Probability of exceedance				DS_m	Damage state
	Slight	Moderate	Severe	Complete		
DSLS4	0.959	0.759	0.397	0.092	2.19	Moderate
DSCP4	0.910	0.613	0.245	0.042	1.82	Moderate
FS4	0.941	0.707	0.333	0.065	2.04	Moderate
DMLS4	0.932	0.660	0.286	0.054	1.94	Moderate
DMCP4	0.917	0.632	0.259	0.046	1.86	Moderate
FM4	0.897	0.583	0.221	0.039	1.76	Moderate
DHLS4	0.855	0.475	0.142	0.019	1.45	Slight
DHCP4	0.836	0.461	0.140	0.017	1.49	Slight
FH4	0.875	0.534	0.186	0.027	1.65	Moderate
DSLS8	0.901	0.592	0.228	0.040	1.78	Moderate
DSCP8	0.908	0.620	0.253	0.044	1.84	Moderate
FS8	0.872	0.528	0.182	0.026	1.63	Moderate
DMLS8	0.867	0.526	0.175	0.025	1.62	Moderate
DMCP8	0.860	0.505	0.166	0.023	1.58	Moderate
FM8	0.827	0.446	0.131	0.016	1.46	Slight
DHLS8	0.698	0.290	0.061	0.005	1.13	Slight
DHCP8	0.710	0.290	0.055	0.005	1.13	Slight
FH8	0.665	0.245	0.045	0.003	1.04	Slight
DSLS15	0.930	0.660	0.280	0.050	1.93	Moderate
DSCP15	0.940	0.710	0.340	0.070	2.07	Moderate
FS15	0.910	0.610	0.250	0.040	1.82	Moderate
DMLS15	0.890	0.580	0.220	0.030	1.75	Moderate
DMCP15	0.910	0.620	0.250	0.040	1.82	Moderate
FM15	0.900	0.590	0.220	0.040	1.78	Moderate
DHLS15	0.870	0.510	0.170	0.020	1.61	Moderate
DHCP15	0.880	0.560	0.200	0.030	1.71	Moderate
FH15	0.850	0.500	0.160	0.020	1.57	Moderate

Table 10 describes the probabilities of surpassing several damage states that can be determined using Fig. 7 represents the probabilities of the predicted damage grade when a chance of 50% is fixed for each damage circumstance. Consider that the performance point of model DSCP15 is 117.26 mm (Table 9) and that the collapse probability of model DSCP15 is calculated to be 7%. (Table 10). The weighted mean damage index (DS_m) is then computed as 1.71 by evaluating the expected probability of exceedance for each damage state (Eqs. 23 and 24). However, based on FEMA P695 (2009) [50] guidelines, all RC frames demonstrate adequate seismic performance, with a collapse risk of less than 10%. (Table 10).

The soils and performance constraints imposed by seismic design have a quantifiable impact on the DS_m on RC frame-building models (Table 10). Even though their outcomes vary, all models created with varied performance requirements and soil conditions exhibit slight to moderate damage. More surveillance is required for 4-storey RC frames constructed on soft soil sites as complete collapse probabilities are high; hence they are more susceptible to seismic damage. The amount of damage detected for structures built on soft soil is between 1.63 and 2.92, whereas for structures built on hard soil, the range is between 1.04 and 1.71. It is noticed that 8-storey RC frames are relatively safe than 4-storey and 15-storey RC frames.

Compared to DDBD-designed structures, FBD-designed structures are shown to be safe in the event of a total collapse, indicating that the code prioritizes greater safety. In contrast, DDBD-designed structures acquire the entire structural capacity according to design-specified requirements and are also seen to be safe. Hence, DDBD gives a cost-effective design that can be implemented according to the relevance of the construction.

Conclusion

The present research is valuable for determining the anticipated damage to RC frame constructions developed with different parameters. The DDBD-designed models are evaluated according to two performance criteria (i)

diverse performance limitations and (ii) distinct soil conditions. The DDBD-designed RC frame models are compared against the FBD technique to determine the efficacy of the DDBD approach. The developed structures are evaluated for nonlinear parameters using multi-mode pushover analysis in MIDAS Gen2021, v3.1 [29]. The seismic assessment of the RC frame models is incorporated by fragility curve generation in a probabilistic manner. The likelihood of exceeding a particular damage state is used to assess the mean damage. Finally, the seismic vulnerability reveals the structure's future damage state regarding the mean damage index. The following are the key conclusions drawn from the study:

- The study observed that the R factor values depend on building height, soil conditions, and performance criteria. R factor values cannot be the same for all building categories, and by modifying the R factor value using this study, more cost-effective structures may be constructed. However, due to inaccuracy in rebar placement, RC frame height, poor quality, and poorer building techniques, the actual values of R for real RC frame constructions may be lower than those calculated in this study.
- While the soil changes from hard to soft, nonlinear analysis reveal that storey drift increases; hence, DDBD has demonstrated effectiveness for various challenges. Moreover, on average, RC frame models on hard soil are slightly damaged, whereas those on medium and soft soil are predicted to experience moderate damage indicating that buildings constructed according to the DDBD method will be economical.
- DDBD-designed buildings adhere to the structure's maximum load capacity following design specifications and are rated safe. However, FBD-constructed structures with higher safety standards but the same strength base design are deemed highly safe. All RC frame models produced using DDBD and FBD have a collapse probability of less than 10% when subjected to seismic forces, indicating a lower likelihood of failure [46]. This study showed that structures exhibit remarkable resilience to massive collapse before failure during an earthquake.

The DDBD approach is helpful for structural design as per their importance, as structures can be designed for required performance criteria. The FBD approach also yields good results but has fixed parameters which can affect structure flexibility and result in more expensive. Further, this study can be extended by considering soil-structure interactions on low-rise, mid-rise, and high-rise buildings using the DDBD approach.

Declarations

Conflict of Interest The authors declares that there is no conflict of interest.

References

1. Priestley MJN, Kowalsky MJ (2000) Direct displacement-based seismic design of concrete buildings. Bull N Z Soc Earthq Eng 33(4):421–441. https://doi.org/10.5459/bnzsee.33.4.421-444
2. FEMA 356. (2000) Prestandard and commentary for the seismic rehabilitation of building. American Society of Civil Engineers (ASCE), Rehabilitation
3. Shibata A, Sozen MA (1976) Substitute-structure method for seismic design in R/C. J Struct Div ASCE 102(12):3548–3566. https://doi.org/10.1016/j.istruc.2021.06.002
4. Medhekar MS, Kennedy DJL (2000) Displacement-based seismic design of buildings - theory. Eng Struct 22(3):201–209. https://doi.org/10.1016/S0141-0296(98)00092-3
5. Pettinga JD, Priestley MJN (2005) Designed with direct displacement-based design. J Earthquake Eng 9(2):309–330. https://doi.org/10.1142/S1363246905002419
6. Aydinoğlu MN (2007) A response spectrum-based nonlinear assessment tool for practice: incremental response spectrum analysis (IRSA). ISET J Earthq Technol 44(1):169–192. https://doi.org/10.1023/A:1024853326383
7. Surmeli M, Yuksel E (2015) A variant of modal pushover analyses (VMPA) based on a non-incremental procedure. Bull Earthq Eng 13(11):3353–3379. https://doi.org/10.1007/s10518-015-9785-3
8. Cardone D, Palermo G, Dolce M (2010) Direct displacement-based design of buildings with different seismic isolation systems. J Earthquake Eng 14(2):163–191. https://doi.org/10.1080/13632460903086036
9. Hu W, Zhang C, Deng Z (2020) Vibration and elastic wave propagation in spatial flexible damping panel attached to four special springs. Commun Nonlinear Sci Num Simulation. https://doi.org/10.1016/j.cnsns.2020.105199
10. Hu W, Deng Z, Han S, Zhang W (2013) Generalized multi-symplectic integrators for a class of Hamiltonian nonlinear wave PDEs. J Comput Phys 235:394–406. https://doi.org/10.1016/j.jcp.2012.10.032
11. Hu W, Xu M, Song J, Gao Q, Deng Z (2021) Coupling dynamic behaviors of flexible stretching hub-beam system. Mech Syst Signal Process 151:107389. https://doi.org/10.1016/j.ymssp.2020.107389
12. Hu W, Wang Z, Zhao Y, Deng Z (2020) Symmetry breaking of infinite-dimensional dynamic system. Appl Math Lett 103:106207. https://doi.org/10.1016/j.aml.2019.106207
13. Hu W, Xu M, Zhang F, Xiao C, Deng Z (2022) Dynamic analysis on flexible hub-beam with step-variable. Mech Syst Signal Proc. https://doi.org/10.1016/j.ymssp.2022.109423
14. Muljati I, Asisi F, Willyanto K (2015) Performance of force based design versus direct displacement based design in predicting seismic demands of regular concrete special moment resisting frames. Proced Eng 125:1050–1056. https://doi.org/10.1016/j.proeng.2015.11.161
15. Sharma A, Tripathi K, R., & Bhat, G. (2020) Comparative performance evaluation of RC frame structures using direct displacement-based design method and force-based design method. Asian J Civil Eng 21(3):381–394. https://doi.org/10.1007/s42107-019-00198-y

16. Giannakouras P, Zeris C (2019) Seismic performance of irregular RC frames designed according to the DDBD approach. Eng Struct 182:427–445. https://doi.org/10.1016/j.engstruct.2018.12.058
17. Qammer SS, Dalal SP, Dalal P (2019) Displacement-based design of RC frames using design spectra of indian code and its seismic performance evaluation. J Inst Eng (Ind) 100(3):367–379. https://doi.org/10.1007/s40030-019-00373-z
18. Kumbhar OG, Kumar R, Farsangi EN (2020) Investigating the efficiency of DDBD approaches for RC buildings. Structures 27(July):1501–1520. https://doi.org/10.1016/j.istruc.2020.07.015
19. Kennedy RP, Cornell CA, Campbell RD, Kaplan S, Perla HF (1980) Probabilistic seismic safety study of an existing nuclear power plant. Nucl Eng Des 59(2):315–338. https://doi.org/10.1016/0029-5493(80)90203-4
20. Dolšek M, Fajfar P (2005) Simplified nonlinear seismic analysis of infilled reinforced concrete frames. Earthquake Eng Struct Dynam 34(1):49–66. https://doi.org/10.1002/eqe.411
21. Choudhury T, Kaushik HB (2018) Seismic fragility of open ground storey RC frames with wall openings for vulnerability assessment. Eng Struct. https://doi.org/10.1016/j.engstruct.2017.11.023
22. Amin, J., Gondaliya, K., & Mulchandani, C. (2021). Assessment of seismic collapse probability of RC shaft supported tank. In *Structures* . Elsevier. DOI: https://doi.org/10.1016/j.istruc.2021.06.002, ISSN: 2352–0124
23. Pan Y, Agrawal AK, Ghosn M (2007) Seismic fragility of continuous steel highway bridges in New York state. J Bridg Eng 12(6):689–699. https://doi.org/10.1061/(asce)1084-0702(2007)12:6(689)
24. Zentner I, Gündel M, Bonfils N (2017) Fragility analysis methods: Review of existing approaches and application. Nucl Eng Des 323:245–258. https://doi.org/10.1016/j.nucengdes.2016.12.021
25. Barbat AH, Pujades LG, Lantada N (2008) Seismic damage evaluation in urban areas using the capacity spectrum method: application to Barcelona. Soil Dyn Earthq Eng 28(10–11):851–865. https://doi.org/10.1016/j.soildyn.2007.10.006
26. IS Is 13920. (2016) Ductile detailing of reinforced Concrete-code of practice. Bureau of Indian Standards, New Delhi, India
27. IS 456. (2000) Indian standard code of practice for plain and Reinforced Concrete. Bureau of Indian Standards, New Delhi, India
28. IS 1893. (2016) Criteria for earthquake resistant design of structures, Part-1 General Provisions and Buildings. Bureau of Indian Standards, New Delhi, India
29. MIDAS Gen (2021). Analysis for civil Structures, 2012:400. URL: https://www.midasstructure.com/en/product/overview/gen
30. Mander JB, Priestley MJ, Park R (1988) Theoretical stress-strain model for confined concrete. J Struct Eng 114(8):1804–1826. https://doi.org/10.1061/(ASCE)0733-9445(1988)114:8(1804)
31. Crespi P, Zucca M, Longarini N, Giordano N (2020) Seismic assessment of six typologies of existing RC bridges. Infrastructures 5(6):52. https://doi.org/10.3390/infrastructures5060052
32. Priestley MJN, Calvi GM, Kowalsky MJ (2007) Displacement-based seismic design of structures. IUSS Press, Pavia
33. IS Is 1893. (2002) Criteria for earthquake resistant design of structures, Part-1 General Provisions and Buildings. Bureau of Indian Standards, New Delhi, India
34. ASCE/SEI 41–17. (2017). Seismic evaluation and retrofit of existing buildings. Reston, Virginia, United States: American society of civil engineers
35. Hu W, Liu T, Han Z (2022) Dynamical symmetry breaking of infinite-dimensional stochastic system. Symmetry 14(8):1–10. https://doi.org/10.3390/sym14081627
36. Chopra AK, Goel RK, Chintanapakdee C (2004) Evaluation of a modified MPA procedure assuming higher modes as elastic to estimate seismic demands. Earthq Spectra 20(3):757–778. https://doi.org/10.1193/1.1775237
37. Chopra AK, Goel RK (2002) A modal pushover analysis procedure for estimating seismic demands for buildings. Earthquake Eng Struct Dynam 31(3):561–582. https://doi.org/10.1002/eqe.144
38. ATC-19. (1996). Structural response modification factors. In *Applied Technology Council*, report ATC-19. Redwood City
39. Gamit K, Amin JA (2021) Drift and response reduction factor of RC frames designed with DDBD and FBD approach. J Inst Eng (India) 102(1):137–151. https://doi.org/10.1007/s40030-020-00488-8
40. Amin, J., & Patel, K. (2019). Assessment of seismic response reduction factor of RC staging elevated water tanks of different staging height. *Indian Concrete J*, 37–48
41. Mulchandani C, Amin J (2021) Assessment of seismic response reduction factor for RC shaft supported tank. J Inst Eng (India) 102(1):75–89. https://doi.org/10.1007/s40030-020-00487-9
42. Gondaliya KM, Amin J, Bhaiya V, Vasanwala S, Desai AK (2023) Seismic vulnerability assessment of indian code compliant rc frame buildings. J Vib Eng Technol 11(1):207–231. https://doi.org/10.1007/s42417-022-00573-1
43. ATC 40. (1996) Seismic Evaluation and Retrofit of Concrete Buildings. Applied Technology Council, Redwood City, CA, USA
44. FEMA P58–1. (2018). Seismic Performance Assessment of Buildings Volume 1 – Methodology Second Edition. *Applied Technology Council*
45. Irizarry J, Lantada N, Pujades LG, Barbat AH, Goula X, Susagna T, Roca A (2011) Ground-shaking scenarios and urban risk evaluation of Barcelona using the Risk-UE capacity spectrum based method. Bull Earthq Eng 9(2):441–466. https://doi.org/10.1007/s10518-010-9222-6
46. Vargas YF, Pujades LG, Barbat AH, Hurtado JE (2013) Capacity, fragility and damage in reinforced concrete buildings: a probabilistic approach. Bull Earthq Eng 11(6):2007–2032. https://doi.org/10.1007/s10518-013-9468-x
47. Lantada N, Irizarry J, Barbat AH, Goula X, Roca A, Susagna T, Pujades LG (2010) Seismic hazard and risk scenarios for Barcelona, Spain, using the Risk-UE vulnerability index method. Bull Earthq Eng 8(2):201–229. https://doi.org/10.1007/s10518-009-9148-z
48. Choudhury T, Kaushik HB (2018) Seismic fragility of open ground storey RC frames with wall openings for vulnerability assessment. Eng Struct 155:345–357
49. HAZUS. (2003). Multi-hazard Loss Estimation Methodology, Earthquake Model, HAZUSMH MR4 Technical Manual. National Institute of Building Sciences and Federal Emergency Management Agency (NIBS and FEMA), Washington, DC
50. Agency FEM (2009) FEMA P695, Quantification of building seismic performance factors. FEMA, Washington